

# $\alpha$ -Glucosidase and Protein Tyrosine Phosphatase 1B Inhibitors from *Malbranchea circinata*

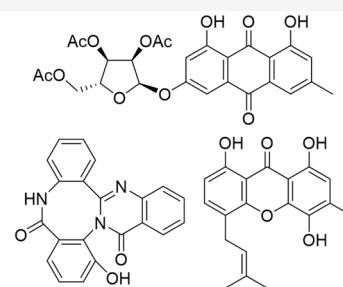
Manuel Rangel-Grimaldo,<sup>†,‡,§</sup> Martha L. Macías-Rubalcava,<sup>†,§</sup> Martin González-Andrade,<sup>§</sup> Huzefa Raja,<sup>||</sup> Mario Figueroa,<sup>†</sup> and Rachel Mata<sup>\*,†,§</sup>

<sup>†</sup>Facultad de Química, <sup>‡</sup>Instituto de Química, and <sup>§</sup>Facultad de Medicina, Universidad Nacional Autónoma de México, Ciudad de México 04510, México

<sup>||</sup>Department of Chemistry and Biochemistry, University of North Carolina Greensboro, Greensboro, North Carolina 27402, United States

## S Supporting Information

**ABSTRACT:** During a search for new  $\alpha$ -glucosidase and protein tyrosine phosphatase 1B inhibitors from fungal sources, eight new secondary metabolites, including two anthranilic acid-derived peptides (1 and 2), four glycosylated anthraquinones (3–6), 4-isoprenylravenelin (7), and a dimer of 5,8-dihydroxy-4-methoxy- $\alpha$ -tetralone (8), along with four known compounds (9–12), were isolated from solid rice-based cultures of *Malbranchea circinata*. The structural elucidation of these metabolites was performed using 1D and 2D NMR techniques and DFT-calculated chemical shifts. Compounds 1–3, 9, and 10 showed inhibitory activity to yeast  $\alpha$ -glucosidase ( $\alpha$ GHY), with  $IC_{50}$  values ranging from 57.4 to 261.3  $\mu$ M ( $IC_{50}$  acarbose = 585.8  $\mu$ M). The effect of 10 (10.0 mg/kg) was corroborated *in vivo* using a sucrose tolerance test in normoglycemic mice. The most active compounds against PTP-1B were 8–10, with  $IC_{50}$  values from 10.9 to 15.3  $\mu$ M ( $IC_{50}$  ursolic acid = 27.8  $\mu$ M). Docking analysis of the active compounds into the crystal structures of  $\alpha$ GHY and PTP-1B predicted that all compounds bind to the catalytic domains of the enzymes. Together, these results showed that *M. circinata* is a potential source of antidiabetic drug leads.



The genus *Malbranchea* contains about 30 species, which are saprotrophic fungi isolated from decaying vegetation, soil, or animal dung worldwide.<sup>1</sup> The members of this genus produce an array of bioactive compounds including eremophilanes,<sup>2</sup> the malbrancheamides,<sup>2–4</sup> a unique family of indole terpenoid alkaloids with vasorelaxant and calmodulin inhibitor properties whose biosynthetic pathway was elegantly elucidated through complementary approaches;<sup>5</sup> pyrrole alkaloids and modified steroids with cytotoxic effects;<sup>6</sup> terpenoids with antifungal, phytotoxic, and cytotoxic activities;<sup>7–9</sup> and polyketides and peptides with antidiabetic properties.<sup>10,11</sup>

According to the International Federation of Diabetes, over the past decade the global prevalence of type-2 diabetes mellitus (T2DM) has nearly quadrupled since 1980, particularly in low- and middle-income countries.<sup>12</sup> In this scenario, it is essential to provide new therapeutic alternatives, including those arising from fungal sources. Hence, we previously reported that assay-guided fractionation of solid-substrate cultures of *Malbranchea flavorosea* led to the isolation of some polyketides and peptide-type compounds with *in vitro* and *in vivo*  $\alpha$ -glucosidase inhibitory properties.<sup>10,11</sup> Here, *Malbranchea circinata* Sigler & Carmichel (Myxotrichaceae) from the American Type Culture Collection (strain no. 34526) was selected for investigation because its rice-based culture

extract showed activity against  $\alpha$ -glucosidases and the protein tyrosine phosphatase 1B (PTP-1B). The latter is critical for insulin signaling due to its ability to dephosphorylate and inactivate the insulin receptor, and inhibition of PTP-1B is an attractive target to improve insulin sensitivity in different cell types.<sup>13–15</sup>  $\alpha$ -Glucosidase inhibitors are currently used in the treatment of patients with T2DM since these agents delay the absorption of carbohydrates from the small intestine and lower the effect on postprandial blood glucose and insulin levels. In this work we describe the isolation and structure elucidation of two anthranilic acid derivatives (1 and 2), four glycosylated anthraquinones (3–6), a prenylated xanthone (7), and a dimer of 5,8-dihydroxy-4-methoxy- $\alpha$ -tetralone (8), along with four known compounds (9–12). All isolates were tested for their inhibitory properties against both  $\alpha$ -glucosidase and PTP-1B.

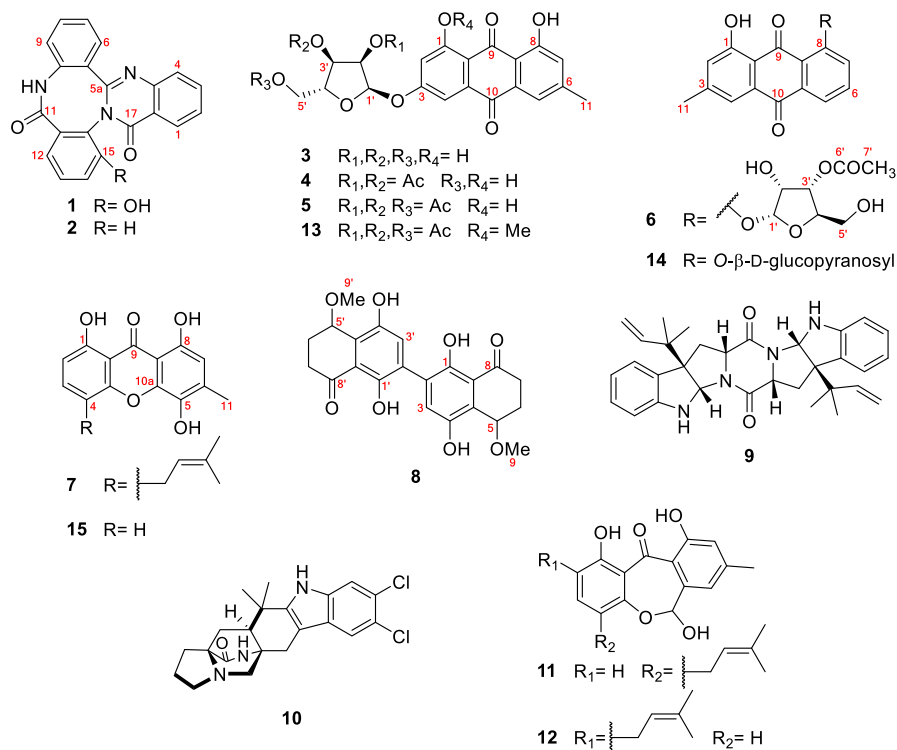
## RESULTS AND DISCUSSION

The defatted extract from moist rice cultures of *M. circinata* inhibited the activity of the  $\alpha$ -glucosidase from yeast ( $IC_{50}$  = 360.7  $\pm$  0.2  $\mu$ g/mL) and PTP-1B ( $IC_{50}$  = 5.3  $\pm$  0.3  $\mu$ g/mL).

**Special Issue:** Special Issue in Honor of Jon Clardy

**Received:** November 7, 2019

Chart 1

Table 1. <sup>1</sup>H (700 MHz) and <sup>13</sup>C (175 MHz) NMR Data of Compounds 1 and 2 in CD<sub>3</sub>OD

position	1				2			
	δ <sub>C</sub>	type	δ <sub>H</sub> , mult. (J in Hz)	HMBC <sup>1</sup> H→ <sup>13</sup> C	δ <sub>C</sub>	type	δ <sub>H</sub> , mult. (J in Hz)	HMBC <sup>1</sup> H→ <sup>13</sup> C
1	126.6	CH	8.31, dd (8.0, 1.5)	3,4,4a,17	126.6	CH	8.32, dd (8.0, 1.5)	3,4a,17
2	127.6	CH	7.65, ddd (8.0, 7.2, 1.5)	4,4a,17,17a	127.7	CH	7.67, ddd (8.0, 7.2, 1.1)	4,4a,17,17a
3	135.0	CH	7.93, ddd (7.6, 7.2, 1.5)	1,4a, 17a	135.1	CH	7.95, ddd (8.3, 7.2, 1.5)	1,4a
4	126.8	CH	7.8, dd (7.6, 1.5)	2,3,4a,17,17a	126.9	CH	7.81, dd (8.3, 1.1)	2,3,17a
4a	147.3	C			147.1	C		
5a	154.5	C			153.8	C		
5b	133.8	C			133.7	C		
6	128.5	CH	7.63, dd (7.6, 1.6)	5a,8,9a	129.0	CH	7.60, dd (7.6, 1.5)	5a,8,9a
7	127.6	CH	7.40, ddd (8.0, 7.6, 1.1)	5b,9	127.7	CH	7.39, ddd (8.0, 7.6, 1.1)	5b,9
8	131.1	CH	7.47, ddd (8.0, 7.6, 1.6)	6,9a	131.1	CH	7.47, ddd (8.0, 7.6, 1.5)	6,9a
9	126.1	CH	7.18, dd (8.0, 1.1)	5a,5b,7	125.9	CH	7.20, dd (8.0, 1.1)	5a,5b,7
9a	136.3	C			136.3	C		
11	170.8	C			170.5	C		
11a	134.2	C			133.3	C		
12	116.9	CH	6.90, dd (7.6, 1.3)	11, 11a	127.3	CH	7.48–7.50, m	11,11a,14
13	130.9	CH	7.29, dd (8.3, 7.6)	11,11a,12,15,15a	129.8	CH	7.48–7.50, m	11a,14
14	117.8	CH	6.92, dd (8.3, 1.3)	12,15,15a	130.8	CH	7.48–7.50, m	12
15	152.6	C			128.2	CH	7.33, m	13
15a	121.7	C			134.1	C		
17	161.0	C			161.7	C		
17a	120.5	C			120.6	C		

Extensive fractionation of the active organic extract led to the isolation of eight new natural products (**1–8**), together with the known compounds amaumine (**9**),<sup>16,17</sup> malbrancheamide (**10**),<sup>3</sup> and the epimeric mixture of arugosin N (**11**) and its C-8 prenyl derivative, 1,6,10-trihydroxy-8-methyl-2-(3-methyl-2-butenyl)dibenz[*b,e*]oxepin-11(6*H*)-one (**12**)<sup>18</sup> (Supporting Information, S1–S51).

Compound **1** was isolated as colorless crystals. Its molecular formula, C<sub>21</sub>H<sub>13</sub>N<sub>3</sub>O<sub>3</sub>, established from the HRESIMS,

indicated an index of hydrogen deficiency (IHD) of 17. The IR spectrum revealed absorptions for amide and aromatic groups (2927, 1684, 1591, and 1566 cm<sup>-1</sup>). Analysis of the <sup>1</sup>H and <sup>13</sup>C NMR data (Table 1 and Figures S1 and S2) indicated the presence of 18 aromatic carbons (11 protonated and seven nonprotonated, one of which was oxygenated), two amide carbonyls, and one imine group. Based on COSY spectra (Figure S5), the 11 protons were part of two 1,2-disubstituted and one 1,2,3-trisubstituted benzene ring. HMBC correlations

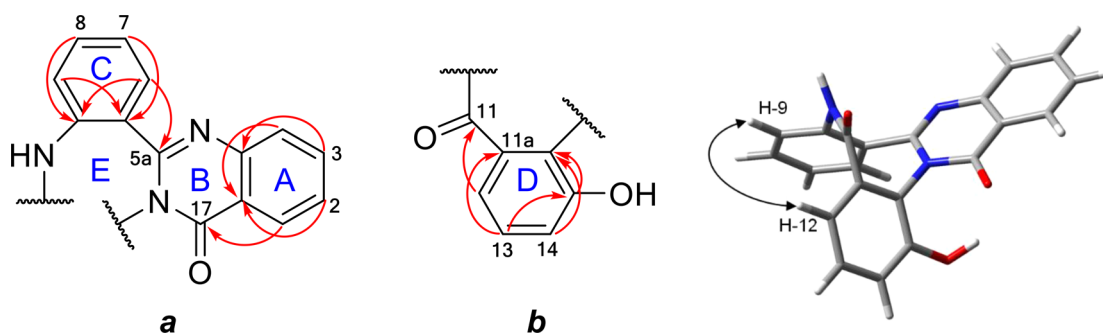


**Figure 1.** Selected key HMBC ( $\rightarrow$ ) correlations of substructures *a* and *b* and NOE ( $\leftrightarrow$ ) correlation between H-9 and H-12 of **1**.

**Table 2.** NMR Data of Compounds 3–5

position	<b>3<sup>a</sup></b>				<b>4<sup>b,c</sup></b>			<b>5<sup>a,c</sup></b>		
	$\delta_C^d$	type	$\delta_{H^1}$ , mult. (J in Hz) <sup>c</sup>	HMBC <sup>d</sup> <sup>1</sup> H $\rightarrow$ <sup>13</sup> C	$\delta_C$	$\delta_{H^1}$ , mult. (J in Hz)	HMBC <sup>1</sup> H $\rightarrow$ <sup>13</sup> C	$\delta_C$	$\delta_{H^1}$ , mult. (J in Hz)	HMBC <sup>1</sup> H $\rightarrow$ <sup>13</sup> C
1	165.0	C			164.8			165.0		
2	109.1	CH	6.97, d (2.5)	1,4	109.8	6.90, d (2.5)	1,4,9a	109.9	6.91, d (2.5)	1,4,9a
3	164.7	C			163.3			163.3		
4	108.2	CH	7.55, d (2.5)	3,4a,10	109.8	7.47, d (2.5)	3,4a,10	110.1	7.48, d (2.5)	3,4a,10
4a	135.0	C			135.2			135.4		
5	120.8	CH	7.67, dq (1.7, 0.7)	7,8a,9,11	121.4	7.62, dq (1.7, 0.9)	7,8a,9,10,11	121.6	7.64, dq (1.7, 0.7)	7,8a,10,11
6	148.8	C			148.7			148.9		
7	124.1	CH	7.13, dq (1.7, 0.7)	5,8,8a,9,11	124.6	7.08, dq (1.7, 0.9)	5,8,8a,11	124.8	7.10, dq (1.7, 0.7)	5,8,8a,9,11
8	161.8	C			162.6			162.8		
8a	113.4	C			113.6			113.8		
9	190.1	C			190.9			191.2		
9a	110.8	C			111.2			111.5		
10	182.4	C			181.8			182.0		
10a	132.9	C			133.1			133.3		
11	21.7	CH <sub>3</sub>	2.48, s		22.2	2.45, s		22.3	2.46, s	
1'	101.8	CH	5.88, d (4.5)	3,3',4'	98.3	6.07, d (4.5)	3,3',4'	98.3	6.04, d (4.5)	3,3',4'
2'	74.7	CH	4.38, dd (6.9, 4.5)	4'	71.2	5.20, dd (7.0, 4.5)	4',2'-COCH <sub>3</sub>	71.0	5.18, dd (7.0, 4.5)	4',2'-COCH <sub>3</sub>
3'	70.5	CH	4.27, m	1',5'	70.0	5.42, m	1',5',3'-COCH <sub>3</sub>	70.0	5.36, m	1',5',3'-COCH <sub>3</sub>
4'	83.9	CH	4.28, m	2',5'	84.2	4.32, m	2',5'	81.4	4.45, m	2',5'
5'	62.7	CH <sub>2</sub>	3.90, m	3',4'	62.0	3.89, dd (12.2, 3.2)	3',4'	63.4	4.34, dd (12.3, 3.2)	3',5'-COCH <sub>3</sub>
			3.81, m	3',4'		3.85, dd (12.2, 3.2)	3',4'		4.26, dd (12.3, 3.2)	3',5'-COCH <sub>3</sub>
2'-COCH <sub>3</sub>					169.9			170.0		
2'-COCH <sub>3</sub>					20.5	2.16, s	2'-COCH <sub>3</sub>	20.9	2.15, s	2'-COCH <sub>3</sub>
3'-COCH <sub>3</sub>					170.6			170.5		
3'-COCH <sub>3</sub>					20.8	2.20, s	3'-COCH <sub>3</sub>	21.0	2.19, s	3'-COCH <sub>3</sub>
5'-COCH <sub>3</sub>								170.6		
5'-COCH <sub>3</sub>								20.6	2.13, s	5'-COCH <sub>3</sub>
1-OH			12.29, s	2,9a		12.23, s	2,9a		12.26, s	2,9a
9-OH			12.09, s	7,8a		12.05, s	7,8a		12.07, s	7,8a

<sup>a</sup><sup>1</sup>H (400 MHz) and <sup>13</sup>C (100 MHz). <sup>b</sup><sup>1</sup>H (700 MHz) and <sup>13</sup>C (175 MHz). <sup>c</sup>CDCl<sub>3</sub>. <sup>d</sup>CDCl<sub>3</sub> + drops of CD<sub>3</sub>OD.

(Figure 1 and Figure S4) and NMR chemical shifts (Table 1) suggested a quinazolinone moiety attached to an aromatic ring (ring C) through the imine carbon (substructure *a*), which is present in a few anthranilic acid alkaloids including sclerotigenin,<sup>19</sup> circumdatin F,<sup>20</sup> asperlicins,<sup>21,22</sup> and benzo-

malvins.<sup>23–25</sup> The protons of ring C (H-6–H-9) showed the following HMBC correlations (Figure 1): H-6 to C-5a, C-8, and C-9a; H-7 to C-5b and C-9; H-8 to C-6 and C-9a; and H-9 to C-7, C-5a, and C-5b. On the other hand, correlations from H-12 to C-11, C-11a, and C-15; H-13 to C-11, C-12, C-15,

and C-15a; and H-14 to C-12 and C-15, as well as the spin system H-12–H-1, typical of a 1,2,3-trisubstituted aromatic ring, supported a 3-hydroxyanthranilic acid residue (sub-structure *b*). Thereby, the extra ring required to fulfill the unsaturation number required by the molecular formula was identified connecting fragments *a* and *b* through C-11 and N-10 and between C-15a and N-16. A NOESY correlation between H-9 and H-12 (distance of 4.3 Å) supported these joining points due to the bending of ring E as observed in the most stable conformation of compound **1** (Figures 1 and S78). Altogether, these data suggest that **1** is a tripeptide formed by two anthranilic acid units and one 3-hydroxyanthranilic acid unit.

Compound **2** was isolated as colorless crystals. Its molecular formula was deduced as C<sub>21</sub>H<sub>13</sub>N<sub>3</sub>O<sub>2</sub> based on the molecular ion peak in the HRESIMS (IHD = 17). Detailed analysis of the 1D and 2D NMR data (Table 1), in particular of the HMBC correlations, indicated that this compound was closely related to **1**: the key differences were observed in ring D, which was disubstituted in compound **2**. Thus, the 1,2,3-trisubstituted benzene ring observed in **1** (protons H-12 to H-14) was replaced by a 1,2-disubstituted aromatic system in **2** (protons H-12 to H-15) (Table 1). Furthermore, a difference of 16 Da and the diamagnetically shifted signal of C-15 from  $\delta_C$  152.6 in **1** to  $\delta_C$  128.2 in **2** suggested that **2** lacks the phenolic group at C-15. Thus, compound **2** was proposed as the 15-deoxy derivative of **1**.

In order to provide further evidence for the NMR structural assignment of **1** and **2**, <sup>1</sup>H and <sup>13</sup>C chemical shifts were calculated and compared with the experimental data. Basically, the protocol involves a conformational search using molecular mechanics, geometry optimization using density functional theory (DFT) with M06-2X/6-31+G(d), and chemical shift calculations using the GIAO method with the B3LYP/6-311+G(2d,p) level of theory.<sup>26,27</sup> Comparisons of computed and experimental NMR chemical shifts of **1** and **2** gave a mean absolute error (MAE) lower than 0.11 ppm for <sup>1</sup>H and lower than 2.0 ppm for <sup>13</sup>C (Tables S3 and S4).

There is no precedent in nature of tripeptides like **1** and **2**. However, it was reported that heating of anthranilic acid with phosphorus pentoxide in refluxing xylene<sup>28</sup> or polyphosphoric acid in an argon current<sup>29</sup> furnished compound **2**. Its UV profile ( $\lambda_{\max}$  280 and 306 nm)<sup>28</sup> was similar to those of **1** and **2** ( $\lambda_{\max}$  280, 306, and 320 nm); however, there are insufficient NMR data available for comparison purposes and we could not duplicate the synthesis of **2**.

Compounds **3–5** were isolated as dark orange glassy solids; their molecular formulas were determined as C<sub>20</sub>H<sub>18</sub>O<sub>9</sub>, C<sub>24</sub>H<sub>22</sub>O<sub>11</sub>, and C<sub>26</sub>H<sub>24</sub>O<sub>12</sub> by HRESIMS (IHD = 12, 14, and 15, respectively). Their NMR spectra (Table 2, Figures S15–S35) were similar to those of 3-*O*-( $\alpha$ -D-ribofuranosyl)-questin (**13**)<sup>30</sup> previously isolated from the endophytic fungus *Eurotium rubrum*. In the case of **3**, the signals due to a methoxy group ( $\delta_H$  3.97, s, OMe-12) in **13** were replaced by resonances for a chelated hydroxy group ( $\delta_H$  12.29, s, OH-1), which was also supported by the difference of 14 Da in their molecular weight. In addition, the <sup>1</sup>H NMR spectrum of **3** showed signals for a second chelated phenolic hydroxy proton at  $\delta_H$  12.09 (OH-9) and for an  $\alpha$ -D-ribofuranosyl unit (Table 2) as in compound **13**. Finally, the HMBC correlation of the anomeric proton at  $\delta_H$  5.88 (d, *J* = 4.5 Hz, H-1') with the signal at  $\delta_C$  164.7 supported the *O*- $\alpha$ -glycosidic linkage to C-3. Acid hydrolysis of **3** afforded ribose, which was identified by TLC

coelution with an authentic sample. The negative optical rotation sign of the monosaccharide was consistent with *D*-ribose.

Based on its NMR data (Table 2 and Figures S15–S35), compounds **4** and **5** showed the same aglycone as **3**; however their ribofuranosyl unit was di- and triacetylated, respectively. Thus, the <sup>13</sup>C and HSQC spectra **4** revealed the presence of two additional carbonyl groups at  $\delta_C$  169.9 (C-6') and  $\delta_C$  170.6 (C-8') and two methyl groups at  $\delta_C$  20.5 (C-7') and  $\delta_C$  20.8 (C-9'). The HMBC connectivities of H-2' to C-4' and 2'-COCH<sub>3</sub>, 2'-COCH<sub>3</sub> to 2'-COCH<sub>3</sub>, H-3' to C-1', C-5', and 3'-COCH<sub>3</sub>, and 3'-COCH<sub>3</sub> to 3'-COCH<sub>3</sub> (Table 2) confirmed the position of the acetyl groups at C-2' and C-3'. The NMR spectra of **5** showed signals for methyl ( $\delta_C$  20.6, 4'-COCH<sub>3</sub>) and a third carbonyl ( $\delta_C$  170.6, 4'-COCH<sub>3</sub>) group, and the HMBC correlations from H-5' to C-4' and 4'-COCH<sub>3</sub> and from 4'-COCH<sub>3</sub> to 4'-COCH<sub>3</sub> indicated that this acyl unit was at C-5' of the carbohydrate moiety. The *D*-monosaccharide configuration of **4** and **5** was assumed on biogenetic grounds.

Compound **6** was isolated as orange glassy solid. Its molecular formula was determined by HRESIMS as C<sub>22</sub>H<sub>20</sub>O<sub>9</sub> (IHD = 13). The NMR data (Table 3 and Figures

**Table 3.** <sup>1</sup>H (700 MHz) and <sup>13</sup>C (175 MHz) NMR Data of Compound **6** in CDCl<sub>3</sub>

position	$\delta_C$	type	$\delta_H$ , mult. ( <i>J</i> in Hz)	HMBC <sup>1</sup> H→ <sup>13</sup> C
1	162.9	C		
2	124.7	CH	7.14, dq (1.8, 0.9)	1,4,9a,11
3	148.4	C		
4	120.6	CH	7.65, dq (1.8, 0.9)	2,9a,10,11
4a	132.4	C		
5	122.0	CH	8.08, dd (7.7, 1.2)	6,7,10
6	136.0	CH	7.78, dd (8.0, 7.7)	5,8,10a
7	122.4	CH	7.70, dd (8.0, 1.2)	5,6,8,8a
8	158.1	C		
8a	121.5	C		
9	189.0	C		
9a	114.9	C		
10	182.4	C		
10a	135.5	C		
11	22.1	CH <sub>3</sub>	2.48, s	2,3,4
1'	102.9	CH	5.85, d (4.4)	8,3',4'
2'	72.0	CH	4.56, m	4'
3'	71.4	CH	5.29, dd (7.0, 2.1)	1',4',5',6'
4'	85.4	CH	4.38, m	2'
5'	62.6	CH <sub>2</sub>	3.91, m	3'
6'	170.8	C		
7'	21.0	CH <sub>3</sub>	2.22, s	6'
1-OH			12.84, s	1,2,3,9a

S36–S42) for this compound were nearly identical to those of known chrysophanein (**14**) (Table 3).<sup>31</sup> However, compound **6** possesses a 3'-acetyl- $\alpha$ -D-ribofuranosyl moiety ( $\delta_H$  5.85, d, *J* = 4.4 Hz, H-1'; 4.56, m, H-2'; 5.29, dd, *J* = 7.0, 2.1 Hz, H-3'; 4.38, m, H-4'; 3.91, m, H-5'; 2.22, s, H<sub>3</sub>-7') rather than the  $\beta$ -D-glucopyranosyl group at C-8. The placement of the ribofuranosyl moiety at C-8 through an *O*-glycosidic linkage was based on the HMBC correlations of the  $\alpha$ -anomeric proton H-1' with C-8 ( $\delta_C$  158.1). On the other hand, HMBC connectivities from H-3' and H-7' to C-6' indicated the position of the acetyl groups at C-3' (Table 3). Therefore,

compound **6** was named chrysophanol *O*-3'-acetyl- $\alpha$ -D-ribofuranoside.

Compound **7** was isolated as a yellow solid. Its molecular formula was deduced as C<sub>19</sub>H<sub>18</sub>O<sub>5</sub>, based on its molecular ion peak in the HRESIMS (IHD = 11). The 1D and 2D NMR data (Table 4 and Figures S43–S49) were consistent with those of

**Table 4.** <sup>1</sup>H (700 MHz) and <sup>13</sup>C (175 MHz) NMR Data of Compound **7** in CDCl<sub>3</sub>

position	$\delta_C$	type	$\delta_H$ , mult. (J in Hz)	HMBC <sup>1</sup> H→ <sup>13</sup> C
1	159.9	C		
2	110.7	CH	6.73, d (8.4)	1,4,9,9a
3	137.7	CH	7.48, d (8.4)	1, 1',4a,9a
4	119.0	C		
4a	153.0	C		
5	134.1	C		
6	135.4	C		
7	111.7	CH	6.64, s	5,8,8a,9,10a
8	153.1	C		
8a	105.8	C		
9	185.9	C		
9a	107.6	C		
10a	142.3	C		
11	16.7	CH <sub>3</sub>	2.41, s	6,7
1'	28.5	CH <sub>2</sub>	3.53, dd (6.8, 1.2)	3,3',4,4',4a,5'
2'	121.9	CH	5.34, m	4,4',5'
3'	133.5	C		
4'	17.9	CH <sub>3</sub>	1.83, s	2',3',5'
5'	25.6	CH <sub>3</sub>	1.81, s	2',3',4'
1-OH			11.85, s	1,2,9a
5-OH			5.15, s	5,6
8-OH			11.03, s	7,8,8a

the 1,4,8-trihydroxy-3-methylxanthone ravenelin (**15**),<sup>32</sup> except for the following key changes: the presence of signals for an isoprene unit ( $\delta_C/\delta_H$  C-1'/H-1', 28.5/3.53; C-2'/H-2', 121.9/5.34; C-3', 133.5; C-4'/H<sub>3</sub>-4', 17.9/1.83; and C-5'/H<sub>3</sub>-5', 25.6/1.81) and two aromatic protons ( $\delta_C/\delta_H$  C-2/H-2, 110.7/6.73, and C-3/H-3, 137.7/7.48) as a pair of *ortho*-coupled doublets. The position of the isoprene unit at C-4 ( $\delta_C$  119.0) was confirmed by the key HMBC correlations from H-1' to C-3, C-4, and C-4a ( $\delta_C$  153.0) and from H-2' to C-4. Moreover, the HMBC correlation from 1-OH to C-1, C-2, and C-9a supported this proposal. On the basis of these considerations, compound **7** was given the trivial name 4-isoprenylravenelin.

Compound **8** (yellow solid) was isolated as a racemic mixture since it was optically inactive, and the CD showed no Cotton effect. The molecular formula was established as C<sub>22</sub>H<sub>22</sub>O<sub>8</sub> according to its HRESIMS peak (IHD = 12). Detailed analysis of the <sup>1</sup>H and <sup>13</sup>C NMR data (Table 5 and Figures S50–S56) indicated that this compound could be a homodimer related to 5,8-dihydroxy-4-methoxy- $\alpha$ -tetralone.<sup>33</sup> The HMBC correlations (Table 5) from H-3 and H-3' to C-1, C-2, C-2', and C-4, and C-1', C-2, C-2', and C-4', respectively; from H<sub>3</sub>-9 and H<sub>3</sub>-9' to C-5 and C-5', respectively; from H-5 and H-5' to C-4a, C-7, and C-9, and C-4a', C-7', and C-9', respectively; from H-6 and H-6' to C-4a, C-5, C-7, and C-8, and C-4a', C-5', C-7', and C-8', respectively; and from H-7 and H-7' to C-5, C-6, and C-8, and C-5', C-6', and C-8', respectively, supported this affirmation. Furthermore, the HMBC connectivities between the chelated phenolic OH-1 and OH-1' to C-1, C-2, and C-8a, and C-1', C-2', and C-8a',

**Table 5.** <sup>1</sup>H (700 MHz) and <sup>13</sup>C (175 MHz) NMR Data of Compound **8** in CDCl<sub>3</sub>

position	$\delta_C$	type	$\delta_H$ , mult. (J in Hz)	HMBC <sup>1</sup> H→ <sup>13</sup> C
1	154.5	C		
2	126.4	C		
3	128.4	CH	7.15, s	1,2,2',4
4	147.0	C		
4a	124.4	C		
5	76.4	CH	4.96, dd (10.5, 4.9)	4a,7,9
6	26.5	CH <sub>2</sub>	2.51, dddd (13.3, 10.5, 4.9, 1.0) 2.21, m	4a,5,7,8 4a,5,7
7	35.5	CH <sub>2</sub>	2.89, ddd (17.5, 12.6, 4.2) 2.62, dddd (17.5, 12.6, 4.2, 1.0)	5,6,8 5,6,8
8	203.2	C		
8a	115.2	C		
9	55.5	CH <sub>3</sub>	3.58, s	5
1'	154.5	C		
2'	126.4	C		
3'	128.4	CH	7.15, s	1',2,2',4'
4'	147.0	C		
4a'	124.4	C		
5'	76.4	CH	4.96, dd (10.5, 4.9)	4a',7',9'
6'	26.5	CH <sub>2</sub>	2.51, ddd (13.3, 10.5, 4.9, 1.0) 2.21, m	4a',5',7',8' 4a',5',7'
7'	35.5	CH <sub>2</sub>	2.89, ddd (17.5, 12.6, 4.2) 2.62, ddd (17.5, 12.6, 4.2, 1.0)	5',6',8' 5',6',8'
8'	203.2	C		
8a'	115.1	C		
9'	55.5	CH <sub>3</sub>	3.58, s	5'
1-OH			12.55, s	1,2,8a
4-OH			7.88, s	3,4
1'-OH			12.54, s	1',2',8a'
4'-OH			7.86, s	3',4'

respectively; and the nonchelated phenolic OH-4 and OH-4' to C-3 and C-4, and C-3' and C-4', respectively, confirmed that the two identical units were linked throughout C-2–C-2'. The conformation of the cyclohexenone ring was determined as a half-chair form on the basis of the NOESY correlation between H-5 and H-5' with one of the methylene protons of H-7 and H-7', respectively; the *J* values of H-7 and H-7' (Table 5) suggested a  $\beta$ - and  $\alpha$ -quasi-axial orientation with respect to the cyclohexenone ring. Interestingly, the chelated and nonchelated phenolic OH groups were not equivalent, probably due to a rotational barrier or the presence of atropoisomerism. Previously, related monomers of **8** were isolated as enantiomeric mixtures from *Juglans mandshurica* Maxim. var. *sieboldiana* Makino (Juglandaceae).<sup>33</sup> In that work, both enantiomers were separated by chiral HPLC, and CD and OR values were obtained. However, the amount of **8** obtained in this work (0.8 mg) precluded separation by this means.

All compounds were evaluated for their inhibitory effects against both  $\alpha$ -glucosidase and PTP-1B. Compounds **1–3**, **9**, and **10** showed inhibitory activity against yeast  $\alpha$ -glucosidase ( $\alpha$ GHY), with IC<sub>50</sub> values of 116.8 ± 7.2, 144.5 ± 4.9, 261.3 ± 7.8, 57.4 ± 0.2, and 71.3 ± 0.7  $\mu$ M, respectively (positive control acarbose, IC<sub>50</sub> = 585.8 ± 0.1  $\mu$ M). The most active compounds, **9** and **10**, were also evaluated against intestinal rat  $\alpha$ -glucosidase enzymes. The calculated IC<sub>50</sub> values were 742.6 ± 7.3 and 458.7 ± 6.6  $\mu$ M, respectively, vs acarbose (IC<sub>50</sub>

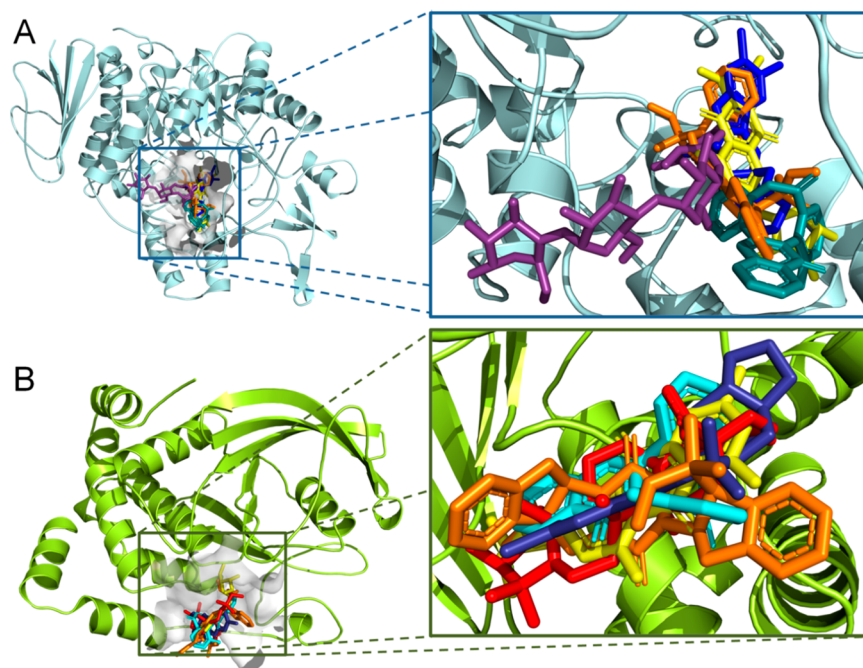


**Figure 2.** Putative binding mode for **1** (cyan sticks), **3** (yellow sticks), **9** (orange sticks), **10** (blue sticks), acarbose (purple sticks), and ursolic acid (red sticks) with (A)  $\alpha$ GHY (skyblue cartoon, pdb code 3A4A) and (B) PTP-1B (green cartoon, pdb code 1SUG).

$151.1 \pm 6.1 \mu\text{M}$ ). The effect of **10** was corroborated *in vivo* using a sucrose tolerance in normoglycemic mice at doses of 3.2 and 10.0 mg/kg. As can be seen in Figure S60, **10** at the dose of 10 mg/kg decreases the postprandial peak in a similar way to that of acarbose (positive control). In order to predict the binding manner of the inhibitors with  $\alpha$ GHY, docking analyses were carried out using the crystallized structure of  $\alpha$ GHY (pdb code 3A4A).<sup>34,35</sup> The docking protocol was validated reproducing the binding mode of acarbose at the catalytic domain,<sup>36</sup> and the results predicted that **1–3**, **9**, and **10** could bind to the catalytic domain (Figure 2 and Figures S61–S65).

Likewise, **1–10** showed moderate inhibitory activity against PTP-1B (Table S5). The most active compounds were **7–10**, with  $\text{IC}_{50}$  values of  $13.9 \pm 1.3$ ,  $10.9 \pm 0.6$ ,  $15.3 \pm 0.4$ , and  $14.5 \pm 1.5 \mu\text{M}$ , respectively (positive control ursolic acid,  $\text{IC}_{50} = 27.8 \pm 0.1 \mu\text{M}$ ). In the same fashion, docking analyses of **7–10** using the crystallized structure of PTP-1B (pdb code 1SUG),<sup>37</sup> validated with ursolic acid,<sup>38</sup> indicated that these compounds bind into the catalytic site (Figure 2 and Figures S66–S74).

In summary, *M. circinata* is a new source of  $\alpha$ -glucosidase and PTP-1B inhibitors that could be useful for the development of antidiabetic drugs. Specifically, malbrancheamide (**10**) possesses vasodilating and antidiabetic effects and holds promise for the design of novel therapies for metabolic syndrome, a cluster of related conditions that increases the risk for developing cardiovascular disease and T2DM.

## EXPERIMENTAL SECTION

**General Experimental Procedures.** IR spectra were recorded using a Bruker Tensor 27 FT-IR spectrophotometer (Bruker Corp., Billerica, MA, USA). Optical rotations were recorded at the sodium D-line wavelength using a PerkinElmer model 343 polarimeter at 20 °C (PerkinElmer, Waltham, MA, USA). NMR spectra were recorded on a Bruker AVANCE III HD with TCI CryoProbe 700 H-C spectrometer at 700 MHz ( $^1\text{H}$ ) or 175 MHz ( $^{13}\text{C}$ ), using tetramethylsilane as an internal standard. High-resolution mass

spectra (HRMS) were acquired with a JEOL AccuTOF-DART JMS-T100LC (JEOL Ltd., Tokyo, Japan) spectrometer in positive mode. Flash chromatography was accomplished on a CombiFlash Rf+ Lumen system (Teledyne Technologies, Inc., Lincoln, NE, USA) using RediSep Rf gold silica gel columns (Teledyne) and eluting with a gradient of *n*-hexane,  $\text{CHCl}_3$ , and MeOH. Analytical and preparative HPLC separations were conducted on Gemini  $\text{C}_{18}$  columns (5  $\mu\text{m}$ , 110 Å, 250  $\times$  4.6 mm i.d. and 5  $\mu\text{m}$ , 110 Å, 250  $\times$  21.2 mm i.d., respectively; Phenomenex, Torrance, CA, USA) in a Waters HPLC system (Waters, Milford, MA, USA) equipped with a 2535 quaternary pump, a 2707 autosampler, and the 2998 PDA and 2424 ELSD detectors. Data management and acquisition were performed with the Empower 3 software (Waters). Column chromatography (CC) was carried out on silica gel 60 (70–230 mesh, Merck, Darmstadt, Germany) or Sephadex LH-20 (GE Healthcare, Chicago, IL, USA). Thin-layer chromatographic (TLC) analyses were performed on silica gel 60  $\text{F}_{254}$  plates (Merck), and visualization of the plates was carried out using a  $(\text{NH}_4)_2\text{Ce}(\text{SO}_4)_4$  (10%) solution in  $\text{H}_2\text{SO}_4$ . Reagent-grade *n*-hexane,  $\text{CHCl}_3$ ,  $\text{CH}_2\text{Cl}_2$ , and MeOH, HPLC-grade MeCN, and  $\text{H}_2\text{O}$  were purchased from J.T. Baker (Avantor Performance Materials, Center Valley, PA, USA).

**Fungal Strain and Identification.** The fungal strain *Malbranchea circinata* Sigler & Carmichael (type strain ATCC 34526)<sup>39</sup> was obtained from the American Type Culture Collection (Manassas, VA, USA). In order to place this fungus into a phylogenetic context and since the type strain was deposited over 40 years ago in the ATCC, we sequenced ATCC 34526 for the ITS rDNA (ITS1, 5.8S and ITS2), as well as the partial 28S rDNA, using primer combinations ITS1F and ITS4<sup>40,41</sup> and LROR and LR6<sup>42,43</sup> using methods outlined previously (Supporting Information).<sup>44</sup> The sequence data are deposited in GenBank with accession numbers ITS: MN627784, MN627785; LSU: MN627782, MN627783.

**Fermentation, Extraction, and Isolation.** *M. circinata* ATCC 34526 was cultivated on potato dextrose agar plates. Seed cultures of the fungus were prepared using agar plugs (0.5  $\text{cm}^3$ ), which were inoculated in potato-dextrose broth (BD, Franklin Lakes, NJ, USA) medium and incubated at room temperature for 10 days at 100 rpm. Next, *M. circinata* was grown in six 2 L Fernbach flasks containing rice medium (200 g and 400 mL of  $\text{H}_2\text{O}$  each). After incubation for 41 days, the cultures were extracted exhaustively with 700 mL of 1:1  $\text{CHCl}_3$ –MeOH. The mixture was shaken for 3 h in a reciprocating

shaker and filtered; then equal volumes of H<sub>2</sub>O and CHCl<sub>3</sub> were added to the filtrate to a total volume of 1 L. After shaking, the mixture was transferred into a separatory funnel and the organic layer was drawn off and evaporated to dryness; the resulting residue was partitioned in a separatory funnel between 180 mL of 1:1 MeOH–MeCN and 180 mL of *n*-hexane, and then the bottom layer was collected and evaporated to dryness. The defatted extract (2.86 g) was dissolved in a mixture of CHCl<sub>3</sub>–MeOH, adsorbed onto a minimal amount of Celite, and fractionated via flash chromatography on a 70 g silica gel column, using a gradient solvent system of *n*-hexane–CHCl<sub>3</sub>–MeOH at a flow rate of 40 mL min<sup>-1</sup> and 35.0 column volumes (CVs) over 109.4 min. Fractions were collected every 23 mL and pooled according to UV and ELSD profiles to obtain 14 fractions (F1–F14).

F1 (121.4 mg) was subjected to silica gel CC eluting with *n*-hexane–CH<sub>2</sub>Cl<sub>2</sub> (75:25 → 0:100) to afford eight fractions (F1<sub>I</sub>–F1<sub>VIII</sub>). From fraction F1<sub>II</sub> (eluted with 75:25 *n*-hexane–CH<sub>2</sub>Cl<sub>2</sub>), 13.9 mg of **6** was obtained. Fraction F1<sub>V</sub> (eluted with 65:35 *n*-hexane–CH<sub>2</sub>Cl<sub>2</sub>) yielded 11.8 mg of the tautomeric mixture of **11** and **12**. F2 (248.6 mg) was first subjected to flash chromatography on a 12 g silica gel column using a gradient solvent system of *n*-hexane–CHCl<sub>3</sub>–MeOH at a flow rate 30 mL min<sup>-1</sup> and 54.0 CVs over 30.2 min, to yield seven fractions (F2<sub>I</sub>–F2<sub>VII</sub>). F2<sub>IV</sub> (146.6 mg) was further purified by preparative RP-HPLC using as mobile phase 65:35 MeCN–H<sub>2</sub>O [0.1% formic acid (FA)] and increasing linearly to 100% MeCN over 15 min, at a flow rate of 21.24 mL min<sup>-1</sup>. This procedure afforded 15.7 mg of **9** (*t*<sub>R</sub> = 8.2 min). F3 (159.1 mg) was purified by silica gel CC with a gradient of *n*-hexane–CH<sub>2</sub>Cl<sub>2</sub>–MeOH (40:60 → 0:100 → 85:15) to afford six fractions (F3<sub>I</sub>–F3<sub>VI</sub>). F3<sub>III</sub> eluted with 25:75 *n*-hexane–CH<sub>2</sub>Cl<sub>2</sub> afforded 23.7 mg of **5**. F5 (86.9 mg) was purified by silica gel CC with a gradient of *n*-hexane–CH<sub>2</sub>Cl<sub>2</sub>–MeOH (30:70 → 0:100 → 70:30) to afford four fractions (F5<sub>I</sub>–F5<sub>IV</sub>). F5<sub>II</sub> eluted with 20:80 *n*-hexane–CH<sub>2</sub>Cl<sub>2</sub> afforded 3.7 mg of **4**. F7 (265.7 mg) was fractionated by flash chromatography on a 12 g silica gel column eluted with a gradient of *n*-hexane–CHCl<sub>3</sub>–MeOH at a 30 mL min<sup>-1</sup> flow rate and 60.3 CVs over 30.2 min, to yield three major fractions (F7<sub>I</sub>–F7<sub>III</sub>). F7<sub>II</sub> (179.4 mg) was purified by preparative RP-HPLC using a gradient of 75:25 MeCN–H<sub>2</sub>O (0.1% FA) and increasing linearly to 100% MeCN in 15 min, at a flow rate of 21.24 mL min<sup>-1</sup>, to obtain 15.9 mg of **10** (*t*<sub>R</sub> = 5.3 min) and 2.0 mg of **2** (*t*<sub>R</sub> = 6.5 min). F8 (215.7 mg) was subject to silica gel CC with a gradient of *n*-hexane–CH<sub>2</sub>Cl<sub>2</sub>–MeOH (20:80 → 0:100 → 70:30). This process yielded 10 fractions (F8<sub>I</sub>–F8<sub>X</sub>). F8<sub>VI</sub> (51.7 mg) was further fractionated via Sephadex LH-20 eluted with 3:7 acetone–MeOH to afford six fractions (F8<sub>VI-A</sub>–F8<sub>VI-F</sub>). F8<sub>VI-B</sub> (7.1 mg) and F8<sub>VI-D</sub> (5.9 mg) were further purified by preparative TLC using 98:2 CHCl<sub>3</sub>–MeOH and 97:3:0.1 CHCl<sub>3</sub>–MeOH–FA as mobile phases, to obtain 1.2 mg of **8** and 1.6 mg of **7**, respectively. Finally, F9 (72.3 mg) was purified by preparative RP-HPLC using a gradient of 70:30 MeCN–H<sub>2</sub>O (0.1% FA) and increasing linearly to MeCN in 12 min, at a flow rate of 21.24 mL min<sup>-1</sup>, to obtain 1.2 mg of **1** (*t*<sub>R</sub> = 5.2 min) and 3.4 mg of **3** (*t*<sub>R</sub> = 6.8 min).

**Compound 1:** white crystalline solid; mp 287 °C; HPLC-UV [(MeCN in H<sub>2</sub>O + 0.1% FA)] λ<sub>max</sub> 280, 306, 320 nm; FTIR ν<sub>max</sub> 2927, 1684, 1591 1566 cm<sup>-1</sup>; <sup>1</sup>H and <sup>13</sup>C NMR see Table 1; HRESIMS *m/z* 356.10324 [M + H]<sup>+</sup> (calcd for C<sub>21</sub>H<sub>14</sub>N<sub>3</sub>O<sub>3</sub> 356.10352).

**Compound 2:** white solid; mp 282 °C; HPLC-UV [(MeCN in H<sub>2</sub>O + 0.1% FA)] λ<sub>max</sub> 280, 306, 320 nm; FTIR ν<sub>max</sub> 2927, 1684, 1591 1566 cm<sup>-1</sup>; <sup>1</sup>H and <sup>13</sup>C NMR see Table 1; HRESIMS *m/z* 340.10942 [M + H]<sup>+</sup> (calcd for C<sub>21</sub>H<sub>14</sub>N<sub>3</sub>O<sub>2</sub> 340.10860).

**Compound 3:** orange glassy solid; UV (MeOH) λ<sub>max</sub> (log ε) 268 (3.66), 225 (3.91) nm; FTIR ν<sub>max</sub> 3330, 2954, 2921, 1628, 1593, 1545 cm<sup>-1</sup>; <sup>1</sup>H and <sup>13</sup>C NMR see Table 2; HRESIMS *m/z* 403.10315 [M + H]<sup>+</sup> (calcd for C<sub>20</sub>H<sub>19</sub>O<sub>9</sub> 403.10291).

**Compound 4:** orange glassy solid; UV (MeOH) λ<sub>max</sub> (log ε) 270 (3.06), 223 (3.22) nm; FTIR ν<sub>max</sub> 3564, 1741, 1630, 1215 cm<sup>-1</sup>; <sup>1</sup>H and <sup>13</sup>C NMR see Table 2; HRESIMS *m/z* 487.12352 [M + H]<sup>+</sup> (calcd for C<sub>24</sub>H<sub>23</sub>O<sub>11</sub> 487.12404).

**Compound 5:** dark orange glassy solid; [α]<sub>D</sub><sup>20</sup> +209.1 (*c* 0.09, CHCl<sub>3</sub>); FTIR ν<sub>max</sub> 3560, 1745, 1677, 1223 cm<sup>-1</sup>; <sup>1</sup>H and <sup>13</sup>C NMR see Table 2; HRESIMS *m/z* 529.13605 [M + H]<sup>+</sup> (calcd for C<sub>26</sub>H<sub>25</sub>O<sub>12</sub> 529.13460).

**Chrysophanol O-3'-acetyl-α-D-ribofuranoside (6):** orange glassy solid; UV (MeOH) λ<sub>max</sub> (log ε) 268 (4.43), 344 (3.99), 405 (3.38) nm; FTIR ν<sub>max</sub> 3450, 1660, 1632, 1582, 1485, 1250, 1226, 1190 cm<sup>-1</sup>; <sup>1</sup>H and <sup>13</sup>C NMR see Table 3; HRESIMS *m/z* 429.11742 [M + H]<sup>+</sup> (calcd for C<sub>22</sub>H<sub>21</sub>O<sub>9</sub> 429.11856).

**4-Isoprenyl ravenelin (7):** dark orange glassy solid; FTIR ν<sub>max</sub> 3560, 1745, 1677, 1223 cm<sup>-1</sup>; <sup>1</sup>H and <sup>13</sup>C NMR see Table 4; HRESIMS *m/z* 327.12308 [M + H]<sup>+</sup> (calcd for C<sub>19</sub>H<sub>19</sub>O<sub>5</sub> 327.12325).

**Compound 8:** yellow glassy solid; [α]<sub>D</sub><sup>20</sup> 0 (*c* 0.08, CHCl<sub>3</sub>); UV (MeOH) λ<sub>max</sub> (log ε) 368 (3.24), 262 (3.59), 228 (3.79), 207 (3.84) nm; FTIR ν<sub>max</sub> 3560, 1745, 1677, 1223 cm<sup>-1</sup>; <sup>1</sup>H and <sup>13</sup>C NMR see Table 5; HRESIMS *m/z* 415.13951 [M + H]<sup>+</sup> (calcd for C<sub>22</sub>H<sub>23</sub>O<sub>8</sub> 415.13929).

**Acid Hydrolysis of Compound 3.** A 2 mg amount of compound **3** dissolved in 1 mL of water was refluxed with 1 mL of HCl (1 M) for 1 h. The reaction mixture was diluted with H<sub>2</sub>O (2 mL) and extracted twice with EtOAc (4 mL). The H<sub>2</sub>O phase was concentrated to dryness to yield α-D-ribofuranoside as detected by TLC with an authentic sample. [α]<sub>D</sub><sup>20</sup> -10 (*c* 0.09, H<sub>2</sub>O).

**Computational Section.** Minimum energy structures for the different structures were built with Spartan'10 software (Wavefunction Inc., Irvine, CA, USA). Conformational analysis was performed with the Monte Carlo search protocol as implemented in the same software under the MMFF94 molecular mechanics force field. The two most stable conformers were submitted to the Gaussian 09 program (Gaussian Inc., Wallingford, CT, USA)<sup>45</sup> calculation for their geometry optimization performed using the M06-2X/6-31+G(d,p) level of theory. The resulting NMR shielding tensors were computed with the gauge-independent atomic orbital (GIAO) method and the polarizable continuum model using the integral equation formalism variant (IEFPCM) as the SCRF method using the DFT method at the B3LYP/6-311+G(2d,p) level of theory.

**Assay for α-Glucosidase Inhibitors.** The fungal extract, fractions, compounds, and acarbose (positive control) were dissolved in MeOH or phosphate buffer solution (PBS, 100 mM, pH 7). Aliquots of 0–10 μL of testing materials (triplicated) were incubated for 10 min with 20 μL of enzyme (Sigma-Aldrich, St. Louis, MO, USA) stock solution (0.4 units/mL) in PBS. After incubation, 10 μL of substrate (pNPG 5 mM) was added and incubated a further 20 min at 37 °C, and the absorbances were determined. For the extract and fractions, the inhibitory activity was determined as percentage in comparison to the blank (PBS) according to the following equation:

$$\% \alpha \text{GHY} = \left( 1 - \frac{A_{415t}}{A_{415c}} \right) \times 100\%$$

where % αGHY is the percentage of inhibition, A<sub>415t</sub> is the corrected absorbance of the extract, fractions, or compound under testing (A<sub>415 end</sub> - A<sub>415 initial</sub>), and A<sub>415c</sub> is the absorbance of the blank (A<sub>415 end blank</sub> - A<sub>415 initial blank</sub>). The IC<sub>50</sub> was calculated by regression analysis, using the following equation:

$$\% \text{Inhibition} = \frac{A_{100}}{1 + \left( \frac{I}{IC_{50}} \right)^s}$$

where A<sub>100</sub> is the maximum inhibition, I is the inhibitor concentration, IC<sub>50</sub> is the concentration required to inhibit activity of the enzyme by 50%, and s is the cooperative degree.

**Expression and Purification of the Enzyme hPTP-1B.** Recombinant hPTP-1B was expressed from the PTPN1 gene (protein tyrosine phosphatase nonreceptor type 1 from *Homo sapiens*, gene ID: 5770). The gene was optimized for overexpression in *E. coli* and subcloned into the pET28 vector to obtain the pET28-PTPN1 system by GenScript (Piscataway, NJ, USA). The overexpression system was transformed into *E. coli* BL21 (DE3) cells with karamycin resistance,

inducing expression with 1 mM of IPTG for 8 h and purifying the enzyme using a His Trap excel column from General Electric. The overexpression and purification process was followed by PAGE-SDS, obtaining a yield of about 90 mg per liter with a purity of 98%.<sup>46</sup>

**Assay for PTP-1B inhibitors.** The fungal extract, fractions, compounds, and positive control were dissolved in DMSO, MeOH, or Tris buffer solution (Tris, 20 mM, pH 7). Aliquots of 0–10  $\mu$ L of testing materials (triplicated) were incubated for 5 min with 20  $\mu$ L of enzyme stock solution (22 nm) in Tris. After incubation, 10  $\mu$ L of substrate (*p*NPP 5 mM) was added and incubated a further 15 min at 25 °C, and the absorbances were determined. For the extract and fractions, the inhibitory activity was determined as percentage in comparison to the blank (Tris) according to the following equation:

$$\%PTP1B = \left(1 - \frac{A_{415t}}{A_{415c}}\right) \times 100\%$$

where % PTP1B is the percentage of inhibition,  $A_{415t}$  is the corrected absorbance of the extract, fractions, or compound under testing ( $A_{415 \text{ end}} - A_{415 \text{ initial}}$ ), and  $A_{415c}$  is the absorbance of the blank ( $A_{415 \text{ end blank}} - A_{415 \text{ initial blank}}$ ). The  $IC_{50}$  was calculated by regression analysis, using the following equation:

$$\%Inhibition = \frac{A_{100}}{1 + \left(\frac{I}{IC_{50}}\right)^s}$$

where  $A_{100}$  is the maximum inhibition,  $I$  is the inhibitor concentration,  $IC_{50}$  is the concentration required to inhibit activity of the enzyme by 50%, and  $s$  is the cooperative degree.

**Sucrose Tolerance Test of Malbrancheamide (10).** ICR male mice 3–4 weeks old (25–30 g body weight) were purchased from Envigo-UNAM. Mice were housed in a room with a 12 h light:dark cycle and controlled for temperature and humidity with free access to standard laboratory rodent diet (Teklad 2018S, Envigo) and water *ad libitum* until the beginning of each experiment. Mice were treated according to the International Ethical Guidelines for the care and use of laboratory animals and following the recommendations of the Mexican Official Norm for Animal Care and Handling (NOM-062-ZOO-1999). The Animal Studies Committee of Facultad de Química, UNAM, approved the experimental protocol (FQ/CICUAL/292/18). After 4 h of food deprivation, mice were divided into five groups (I–V) of six animals each. The animals of group I were administered with VEH (saline solution with 0.05% Tween 80) and group II with reference drug (acarbose 5 mg/kg). Groups III–V were treated orally with **10** at the doses of 3.1 and 10 mg/kg. Thirty minutes later, sucrose (3 g/kg) was orally administered to each animal. Blood glucose concentrations were determined at 30, 60, 90, and 120 min postadministration of the carbohydrate load. The percentage of glycemic variation (%) was determined with respect to the basal level as follows:

$$\%variation \text{ of glycemia} = \left[\frac{(G_t - G_i)}{G_i}\right] \times 100$$

where  $G_i$  is the basal glycemia and  $G_t$  is the different glycemia values after treatment administration.<sup>10,47</sup>

**Docking Studies.** The minimized structures for docking simulations were prepared using Autodock Tools package v1.5.4 (ADT, <http://mglttools.scripps.edu/>).<sup>48</sup> For metabolites, addition of Gasteiger charges and number of torsions were set, and nonpolar hydrogens were merged. The crystallographic structure of  $\alpha$ -glucosidase from yeast and PTP-1B from human was obtained from the Protein Data Bank (pdb code 3A4A and 1SUG, respectively). For the receptor polar hydrogens and Kollman charges were added, and solvation parameters were assigned by default. Molecular docking studies were achieved with AutoDock v1.1.2.15. First, a blind docking was performed in order to establish the common site of interaction of the metabolites with the  $\alpha$ -glucosidase and PTP1B. The search space for this preliminary docking was defined as a box size of 90  $\times$  90  $\times$  90 Å in the  $x$ ,  $y$ , and  $z$  dimensions, with a grid spacing of 0.375 Å, and the

macromolecule was set as the center of the box. The default parameters of exhaustiveness and number of modes were not altered. Next, a refined docking was performed with a smaller box of searching space (50  $\times$  50  $\times$  50 and 0.375 Å of grid spacing), setting as the center of the grid box the lower state pose obtained from the blind docking. The conformational states from the docking simulations were analyzed using the AutoDockTools program, which also identified the H-bonds and van der Waals interactions between the catalytic site of  $\alpha$ -glucosidase or PTP1B and the ligand. The predicted docked complexes (protein–ligand) were those conformations showing the lowest binding energy. Preparation of the figures was accomplished with the PyMOL visualization tool (PyMOL Molecular Graphics System v1.7.4, Schrödinger, New York, NY, USA<sup>49,50</sup> and Maestro (Schrödinger)).<sup>51</sup>

## ■ ASSOCIATED CONTENT

### 📄 Supporting Information

The Supporting Information is available free of charge at <https://pubs.acs.org/doi/10.1021/acs.jnatprod.9b01108>.

1D and 2D NMR spectra of **1–8** and <sup>1</sup>H NMR of **9–12**; phylograms of the most likely tree based on the analyses of the ITS and LSU regions; docking analyses showing the interactions of the active compounds with  $\alpha$ -glucosidase and PTP-1B (PDF)

## ■ AUTHOR INFORMATION

### Corresponding Author

\*Tel: +52-55-5622-5289. E-mail: [rachel@unam.mx](mailto:rachel@unam.mx).

### ORCID

Manuel Rangel-Grimaldo: 0000-0003-1261-3317

Martha L. Macías-Rubalcava: 0000-0001-9650-0920

Martin González-Andrade: 0000-0002-8910-3035

Huzefa Raja: 0000-0002-0824-9463

Mario Figueroa: 0000-0001-7004-0591

Rachel Mata: 0000-0002-2861-2768

### Author Contributions

<sup>‡</sup>Taken in part from the Ph.D. thesis of Manuel Rangel-Grimaldo.

### Notes

The authors declare no competing financial interest.

## ■ ACKNOWLEDGMENTS

This work was supported by grants from CONACyT CB A1-S-11226 and DGAPA IN 217320. M.R.G. acknowledges the fellowship from CONACYT (294309) to pursue graduate studies. This study made use of UNAM's NMR lab, LURMN at IQ-UNAM, which is funded by CONACYT-0224747, and UNAM. The authors also recognize the valuable support of I. Rivero-Cruz and A. Vázquez-Pérez from Facultad de Química, M. I. Velásquez-López from Facultad de Medicina, and B. Quiroz García, M. A. Peña González, E. Huerta Salazar, J. Pérez Flores, M. C. García-González, and R. Patiño Maya from Instituto de Química, for recording NMR, IR, UV, and MS spectra. We are indebted to Dirección General de Cómputo y de Tecnologías de Información y Comunicación (DGTIC), UNAM, for the resources to carry out computational calculations through the Miztli supercomputing system (LANCAD-UNAM-DGTIC-313).

## ■ DEDICATION

Dedicated to Dr. Jon Clardy of Harvard Medical School for his pioneering work on bioactive natural products.

## ■ REFERENCES

- (1) Mata, R.; Figueroa, M.; Rivero-Cruz, I.; Macías-Rubalcava, M. L. *Planta Med.* **2018**, *84*, 594–605.
- (2) Martínez-Luis, S.; González, M. C.; Ulloa, M.; Mata, R. *Phytochemistry* **2005**, *66*, 1012–1016.
- (3) Martínez-Luis, S.; Rodríguez, R.; Acevedo, L.; González, M. C.; Lira-Rocha, A.; Mata, R. *Tetrahedron* **2006**, *62*, 1817–1822.
- (4) Figueroa, M.; González, M. D. C.; Mata, R. *Nat. Prod. Res.* **2008**, *22* (8), 709–714.
- (5) Miller, K. A.; Welche, T. R.; Greshock, T. J.; Ding, Y.; Sherman, D. H.; Williams, R. M. *J. Org. Chem.* **2008**, *73*, 3116–3119.
- (6) Yang, Y. L.; Liao, W. Y.; Liu, W. Y.; Liaw, C. C.; Shen, C. N.; Huang, Z. Y.; Wu, S. H. *Chem. - Eur. J.* **2009**, *15*, 11573–11580.
- (7) Wakana, D.; Itabashi, T.; Kawai, K. I.; Yaguchi, T.; Fukushima, K.; Goda, Y.; Hosoe, T. *J. Antibiot.* **2014**, *67*, 585–588.
- (8) Wakana, D.; Hosoe, T.; Wachi, H.; Itabashi, T.; Fukushima, K.; Yaguchi, T.; Kawai, K. I. *J. Antibiot.* **2009**, *62*, 217–219.
- (9) Wakana, D.; Hosoe, T.; Itabashi, T.; Fukushima, K.; Kawai, K. *Mycotoxins* **2008**, *58*, 1–6.
- (10) Verastegui-Omaña, B.; Rebolgar-Ramos, D.; Pérez-Vásquez, A.; Martínez, A. L.; Madariaga-Mazón, A.; Flores-Bocanegra, L.; Mata, R. *J. Nat. Prod.* **2017**, *80*, 190–195.
- (11) Rebolgar-Ramos, D.; Macías-Rubalcava, M. L.; Figueroa, M.; Raja, H. A.; González-Andrade, M.; Mata, R. *J. Antibiot.* **2018**, *71*, 862–871.
- (12) International Diabetes Federation. *IDF Diabetes Atlas*, 9th ed.; International Diabetes Federation: Brussels, Belgium, 2019. <http://diabetesatlas.org>.
- (13) Ezzat, S. M.; El Bishbishy, M. H.; Habtemariam, S.; Salehi, B.; Sharifi-Rad, M.; Martins, N.; Sharifi-Rad, J. *Molecules* **2018**, *23*, 3334–3362.
- (14) Tamrakar, A. K.; Maurya, C. K.; Rai, A. K. *Expert Opin. Ther. Pat.* **2014**, *24*, 1101–1115.
- (15) Zhang, Z. Y.; Lee, S. Y. *Expert Opin. Invest. Drugs* **2003**, *12*, 223–233.
- (16) Takase, S.; Kawai, Y.; Uchida, I.; Tanaka, H.; Aoki, H. *Tetrahedron* **1985**, *41*, 3037–3048.
- (17) Elsebai, M. F.; Rempel, V.; Schnakenburg, G.; Kehraus, S.; Müller, C. E.; König, G. M. *ACS Med. Chem. Lett.* **2011**, *2*, 866–869.
- (18) Sun, T. Y.; Kuang, R. Q.; Chen, G. D.; Qin, S. Y.; Wang, C. X.; Hu, D.; Wu, B.; Liu, X. Z.; Yao, X. S.; Gao, H. *Molecules* **2016**, *21*, 1184–1196.
- (19) Witt, F. A.; Bergman, J. J. *Heterocycl. Chem.* **2002**, *39*, 351–355.
- (20) Rahbæk, L.; Breinholt, J. *J. Nat. Prod.* **1999**, *62*, 904–905.
- (21) Xu, Y.-J.; Pieters, L. *Mini-Rev. Med. Chem.* **2013**, *13*, 1056–1072.
- (22) Tseng, M. C.; Yang, H. Y.; Chu, Y. H. *Org. Biomol. Chem.* **2010**, *8*, 419–427.
- (23) Sun, H. H.; Barrow, C. J.; Sedlock, D. M.; Gillum, A. M.; Cooper, R. *J. Antibiot.* **1994**, *47*, 515–522.
- (24) Clevenger, K. D.; Ye, R.; Bok, J. W.; Thomas, P. M.; Islam, M. N.; Miley, G. P.; Robey, M. T.; Chen, C.; Yang, K.; Swyers, M.; Wu, E.; Gao, P.; Wu, C. C.; Keller, N. P.; Kelleher, N. L. *Biochemistry* **2018**, *57*, 3237–3243.
- (25) Jang, J. P.; Jang, J. H.; Soung, N. K.; Kim, H. M.; Jeong, S. J.; Asami, Y.; Shin, K. S.; Kim, M. R.; Oh, H.; Kim, B. Y. *J. Antibiot.* **2012**, *65* (4), 215–217.
- (26) Willoughby, P. H.; Jansma, M. J.; Hoye, T. R. *Nat. Protoc.* **2014**, *9*, 643–660.
- (27) Lodewyk, M. W.; Siebert, M. R.; Tantillo, D. J. *Chem. Rev.* **2012**, *112*, 1839–1862.
- (28) Chatterjee, A.; Ganguly, M. *J. Org. Chem.* **1968**, *33*, 3358.
- (29) Siling, S. A.; Ponomarev, I. I. *Bull. Acad. Sci. USSR, Div. Chem. Sci.* **1978**, *27*, 1643–1649.
- (30) Li, D. L.; Li, X. M.; Wang, B. G. *J. Microbiol. Biotechnol.* **2009**, *19*, 675–680.
- (31) Kubo, I.; Murai, Y.; Soediro, I.; Soetarno, S.; Sastrodihardjo, S. *Phytochemistry* **1992**, *31*, 1063–1065.
- (32) van Eijk, G.; Gerbertus, W.; Roeymans, H. *Exp. Mycol.* **1981**, *5*, 373–375.
- (33) Machida, K.; Matsuoka, E.; Kasahara, T.; Kikuchi, M. *Chem. Pharm. Bull.* **2005**, *53* (8), 934–937.
- (34) Morris, G. M.; Goodsell, D. S.; Halliday, R. S.; Huey, R.; Hart, W. E.; Belew, R. K.; Olson, A. J. *J. Comput. Chem.* **1998**, *19*, 1639–1662.
- (35) Rudnitskaya, A.; Török, B.; Török, M. *Biochem. Mol. Biol. Educ.* **2010**, *38*, 261–265.
- (36) Yamamoto, K.; Nakayama, A.; Yamamoto, Y.; Tabata, S. *Eur. J. Biochem.* **2004**, *271*, 3414–3420.
- (37) Pedersen, A. K.; Peters, G. H.; Møller, K. B.; Iversen, L. F.; Kastrup, J. S. *Acta Crystallogr., Sect. D: Biol. Crystallogr.* **2004**, *60* (9), 1527–1534.
- (38) Jiang, C. S.; Liang, L. F.; Guo, Y. W. *Acta Pharmacol. Sin.* **2012**, *33*, 1217–1245.
- (39) Sigler, L.; Carmichael, J. W. *Mycotaxon* **1976**, *4*, 349–488.
- (40) White, T. J.; Bruns, T.; Lee, S.; Taylor, J. W. *PCR Protocols: a Guide to Methods and Application*; Academic Press: San Diego, 1990; pp 315–322.
- (41) Gardes, M.; White, T. J.; Fortin, J. A.; Bruns, T. D.; Taylor, J. W. *Can. J. Bot.* **1991**, *69*, 180–190.
- (42) Vilgalys, R.; Hester, M. *J. Bacteriol.* **1990**, *172*, 4283–4286.
- (43) Rehner, S. A.; Samuels, G. J. *Can. J. Bot.* **1995**, *73*, 816–823.
- (44) Raja, H. A.; Miller, A. N.; Pearce, C. J.; Oberlies, N. H. *J. Nat. Prod.* **2017**, *80*, 756–770.
- (45) Frisch, M. J.; Trucks, G. W.; Schlegel, H. B.; Scuseria, G. E.; Robb, M. A.; Cheeseman, J. R.; Scalmani, G.; Barone, V.; Mennucci, B.; Petersson, G. A.; Nakatsuji, H.; Caricato, M.; Li, X.; Hratchian, H. P.; Izmaylov, A. F.; Bloino, J.; Zheng, G.; Sonnenberg, J. L.; Hada, M.; Ehara, M.; Toyota, K.; Fukuda, R.; Hasegawa, J.; Ishida, M.; Nakajima, T.; Honda, Y.; Kitao, O.; Nakai, H.; Vreven, T.; Montgomery, J. A., Jr.; Peralta, J. E.; Ogliaro, F.; Bearpark, M.; Heyd, J. J.; Brothers, E.; Kudin, K. N.; Staroverov, V. N.; Keith, T.; Kobayashi, R.; Normand, J.; Raghavachari, K.; Rendell, A.; Burant, J. C.; Iyengar, S. S.; Tomasi, J.; Cossi, M.; Rega, N.; Millam, J. M.; Klene, M.; Knox, J. E.; Cross, J. B.; Bakken, V.; Adamo, C.; Jaramillo, J.; Gomperts, R.; Stratmann, R. E.; Yazyev, O.; Austin, A. J.; Cammi, R.; Pomelli, C.; Ochterski, J. W.; Martin, R. L.; Morokuma, K.; Zakrzewski, V. G.; Voth, G. A.; Salvador, P.; Dannenberg, J. J.; Dapprich, S.; Daniels, A. D.; Farkas, O.; Foresman, J. B.; Ortiz, J. V.; Cioslowski, J.; Fox, D. J. *Gaussian 09*, Revision E.01; Gaussian, Inc.: Wallingford, CT, 2013.
- (46) Puius, Y. A.; Zhao, Y.; Sullivan, M.; Lawrence, D. S.; Almo, S. C.; Zhang, Z. Y. *Proc. Natl. Acad. Sci. U. S. A.* **1997**, *94*, 13420–13425.
- (47) Lozano-González, M.; Ovalle-Magallanes, B.; Rangel-Grimaldo, M.; De La Torre-Zavala, S.; Noriega, L. G.; Tovar-Palacio, C.; Tovar, A. R.; Mata, R. *New J. Chem.* **2019**, *43*, 7756–7762.
- (48) Morris, G. M.; Huey, R.; Lindstrom, W.; Sanner, M. F.; Belew, R. K.; Goodsell, D. S.; Olson, A. J. *J. Comput. Chem.* **2009**, *30*, 2785–2791.
- (49) *The PyMOL Molecular Graphics System, Version 2.1.1*; Schrödinger, 2015.
- (50) Seeliger, D.; De Groot, B. L. *J. Comput.-Aided Mol. Des.* **2010**, *24*, 417–422.
- (51) Schrödinger Release 2019-3: *Maestro*; Schrödinger, LLC: New York, NY, 2019.